IEEE Access
Multidisciplinary | Rapid Review | Open Access Journal

Received May 30, 2020, accepted July 18, 2020, date of publication August 6, 2020, date of current version August 20, 2020.

Digital Object Identifier 10.1109/ACCESS.2020.3014643

A Detailed Thermal and Effective Induced Residual Spin Rate Analysis for LEO Small Satellites

ANWAR ALI[1], JIJUN TONG[1], HAIDER ALI[2], (Senior Member, IEEE), MUHAMMAD RIZWAN MUGHAL[3,4], AND LEONARDO M. REYNERI[5]

[1]School of Information Science and Technology, Zhejiang Sci-Tech University, Hangzhou 310018, China
[2]Department of Electrical Engineering Technology, University of Technology (UoT), Nowshera 24100, Pakistan
[3]Department of Electronics and Nanoengineering, School of Electrical Engineering, Aalto University, 02150 Espoo, Finland
[4]Department of Electrical Engineering, Institute of Space Technology, Islamabad 44000, Pakistan
[5]Department of Electronics and Telecommunication (DET), Politecnico di Torino, 10129 Turin, Italy

Corresponding author: Jijun Tong (jijuntong@zstu.edu.cn)

ABSTRACT In space thermal environment, satellites are exposed to multiple heat sources which can deteriorate structural and equipment integrity over long periods of time. Normally radiators are used to release heat, but due to space and weight constraints, it is impossible to mount radiators on small satellites. This problem signifies the importance of thermal analysis of a satellite in every development stage, such as design, manufacturing and testing. The ultimate goal of this work is to analyze a small spacecraft in space thermal environment by considering the effect of various heat sources. Thermal equilibrium equation is achieved which is applied to spacecraft with different shapes and dimensions and temperature is measured for a range of absorption co-efficient values (i.e. $0.5 \sim 0.9$). Through an experimental setup a method is devised to measure the absorption co-efficient of small satellites that can be used for exact temperature measurement. Secondly, the paper presents a preliminary analysis of induced spin produced by small satellites due to asymmetrical colors (different absorptance) of satellite outer surface. The substantial contributors for induced spin are considered and the estimated spin is measured.

INDEX TERMS Satellites, thermal analysis, temperature, absorption.

I. INTRODUCTION

Recently, there is a great emphasis on the development of small satellites by universities and SMEs (small and medium enterprisers) because they are simple, cheaper and easy to launch [1], [2]. In this regard, the first NanoSatellite was developed in 1999 by California Polytechnic State University (Cal Poly) in collaboration with Stanford University, called CubeSat with dimensions $10 \times 10 \times 10$ cm^3 [3], [4]. This provided a new research area to universities and SMEs worldwide in the field of small satellites. Department of Electronics and Telecommunication (DET) at Politecnico di Torino is also working on a comprehensive NanoSatellite project called AraMiS [5], designing small satellites for Low Earth Orbit (LEO). The design process of AraMiS is based on the concept of tiles [6] and modules. The tiles and modules have different dimensions and technology to achieve any desired satellite structure. These modules can be reused for multiple missions that help in significant reduction of the overall budget, design, development and testing time. One has to reassemble the required modules to achieve the specific targeted mission. This architecture is intended for different satellite missions, from small systems weighing from 1kg to larger missions weighing up to 50 kg. Fig. 1 and Fig. 2 depict a number of AraMiS satellites and its modular subsystems respectively that show the potential capabilities of the proposed concept [1]. Modularity and redundancy have been implemented in different ways. From the mechanical perspective, larger satellite structures can be conveniently realized by combining several small modular structures. The modularity concept has also been intended from electronic standpoint. Most of the internal subsystems are developed in such a manner that they can be combined together to enhance performance and develop a new subsystem [7].

The associate editor coordinating the review of this manuscript and approving it for publication was Md. Moinul Hossain.

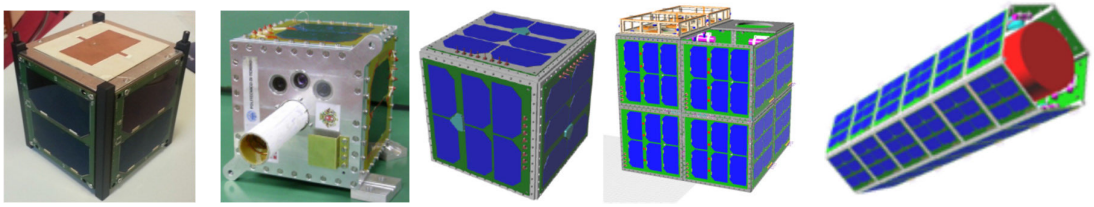

FIGURE 1. Various AraMiS architectures (a) AraMiS-C1 (b) PiCPoT (c) AraMiS-C2 (d) 8U-AraMiS-C2 (e) Hexagonal Prism.

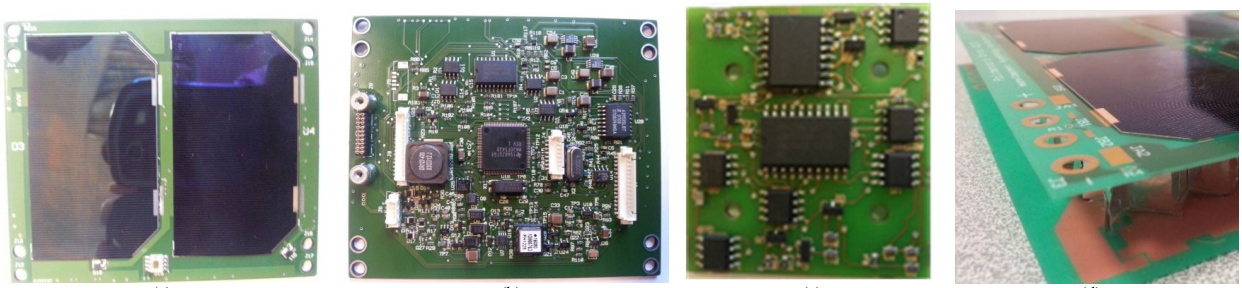

FIGURE 2. AraMiS modular subsystems (a) Solar panel of CubePMT (b) Component side of CubePMT (c) Magnetometer Unit (d) Honeycomb Structure.

The first NanoSatellite based on the modular architecture of AraMiS project is AraMiS-C1, which is modular at electrical, mechanical and software levels. In this architecture, major tasks are divided over a number of identical modules that are developed in a tile (integrated inside the same PCB) which makes the design, development, testing and integration very simple. The modules communicate data and power in a distributed and self-configuring manner, which has standardized interfaces among various subsystems. Out-dated products can be replaced with enhanced modular systems without affecting the remaining satellite subsystem [8].

Four sides of AraMiS-C1 are equipped with identical ''tiles'' called CubePMT [10, 11]. CubePMT is developed on a single eight layers PCB with dimensions 82.5 × 98× 1.6 mm^3. The top side (Layer-1) has two solar cells and sun sensor while the bottom side (Layer-8) contains all the electronic subsystems as shown in Fig. 2(a) and Fig. 2(b). Magnetorquer coil with 200 turns is integrated inside the PCB four internal layers (layer 2, 3, 4 & 5) as shown in Fig. 3. The other two sides are devoted to the telecommunication links and carry a commercial deployable UHF antenna (one side) and a patch type SHF antenna (the other side) on the exterior.

In space thermal environment, one of the major problems with small satellites is to dissipate extra heat because they are exposed to many heat sources which continuously increase the satellite temperature [11]. Normally for heat removal radiators are mounted on spacecraft, but due to space and weight constraints of small satellites, embedding radiators are incompatible with them [12]. The design phase of any spacecraft requires a preliminary thermal analysis, in order to evaluate the spacecraft and provide the

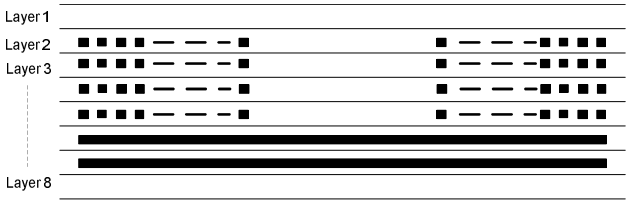

FIGURE 3. CubePMT internal layers view.

temperature details that whether the spacecraft will remain within the operational temperature limits or not. Preliminary thermal and spin analysis give a freedom to the designer on spacecraft dimension, mass, orbital parameters and material thermo-optical properties (i.e. emissivity & absorptance etc.).

Heat is generated by the satellite subsystem as well as absorbed from the environment. Components generating heat are electronic devices, motors and batteries. Heat from the environment is mainly due to solar radiation [13]. Thus satellite thermal control requires the selection of suitable structural material and devices that should maintain a balance between heat absorbed and emitted to the environment.

Spacecraft is exposed to harsh space thermal environment as soon as it is launched [14]. During cold space environment, heaters are used to keep the satellite subsystems above the acceptable temperature limits. However during hot space condition, small satellite has no coolers to keep the subsystems temperature under the permissible temperature limits [15]. The only choice for small satellites is the balance thermal control design which adopts passive thermal control systems [16]. Therefore it is significant to know the space

environment heat sources and design the satellite according to the space thermal conditions.

A number of efforts were made to analytically solve the thermal equilibrium equation of a satellite [17], [18]. In [19], for the spacecraft thermal analysis, the author is using the lumped parameter model. According to the author, the entire system can be divided into various numbers of nodes, where every node is isothermal which represents the thermal characteristics of its surrounding medium. The main problem in this technique is that better accuracy can be achieved at the cost of complexity. In [20], the author presented a closed-form prediction model for the temperature distribution of a thick-walled cylindrical spinning satellite subjected to solar heating in deep space. This is not straight forward due to the complexity of the necessary calculations. In [21], a revised hima's model for the spacecraft thermal analysis was presented, but the problem with this modeling technique is that the results are very complex and not easy to apply for thermal calculation purposes. In [22], Assal and Asabel presented a simplified analysis of the thermal behavior of a spinning satellite, orbiting the Earth over Sun-synchronous orbits. In this work the analysis was conducted by linearizing the equations about their equilibrium points and studying the influence of the averaged external heat loads and the periodic parts separately. Again the complexity and assumptions for linearization make the model inaccurate and inappropriate. In [23], the differential non-linear equations of heat transfer are linearized and applied to the thermal analysis of small satellites in LEO. This technique is based on theoretical mathematical modeling where no laboratory measurements of practical cases are considered. The edge of our technique over the others is the capability of predicting the spacecraft temperature using the aerospace environment parameters and ordinary laboratory equipment i.e. vacuum chamber, data acquisition system, oscilloscope etc. No specific software or specialized laboratory equipment is required which are very expensive and not easily available. It is a very quick, easily repeatable and very cheap method for spacecraft thermal analysis in the aerospace environment. In this work, all the possible heat sources are considered which are faced by a small satellite during revolving around the Earth and a thermal balance equation is derived. Various dimension spacecraft structures are analysed in thermal equilibrium under different conditions through diverse cases. In all these cases, the generated heat is plotted against the temperature rise of the space-crafts for a range of emissivity values (0.5 $\sim$ 0.9). A technique is developed that how the emissivity of a spacecraft is found which can be used for accurate temperature measurement. Preliminary analysis of induced spin by the color (absorptance) asymmetry of the satellite outer surface is performed.

The paper is structured as follows. In section 2, spacecraft is analysed in space thermal environment. As various heat sources are encountered by the satellite during orbiting the earth, therefore a thermal equilibrium equation is derived in this section by considering all the thermal sources. Section 3 presents a profound thermal analysis of various dimension spacecraft's structure in thermal equilibrium under different conditions. These conditions are explained through different cases. In section 4, a technique is devised that how the emissivity of a panel body can be measured where the emissivity of the AraMiS satellite solar panel is found. Section 5 of the paper presents a preliminary analysis of an ARAMIS dimension system in relation to the spin induced by the color (thermal absorptance) asymmetry of the satellite outer surface. Finally, section 6 concludes the paper.

II. SPACECRAFT THERMAL ANALYSIS IN SPACE ENVIRONMENT

During orbiting the earth, a small satellite encounters several heat sources considering substantial contributions due to:

i. Solar radiation which depends on the sun distance, with a mean value around 1366 W/m^2 [24]
ii. The Earth albedo reflected radiation with mean reflectivity around 30% which varying up to 40 to 80% above shiny clouds and from 5% to 10% for ocean and forests [24]
iii. Thermal terrestrial radiation for which the earth can be modelled as an equivalent black-body emitting at 255K [25]
iv. Heating due to internal heat generation in electronic components (Joule's effect) [26]
v. Heat capacity of the system [27]
vi. Cooling due to heat radiation
vii. Cooling due to the conversion of solar energy into electricity

The satellite temperature periodically varies along its orbit. During eclipse, only two heat sources are present; thermal terrestrial radiation and internal heat generation in electronic components. Therefore the satellite is cooler during the eclipse and hotter in sunshine. The system is considered to be completely isothermal. Before going into further thermal analysis details, we propose some preconditions.

A. PRECONDITIONS

Let consider a system composed of N isothermal faces oriented in space with each face characterized by an absorptance (α); $0 < \alpha < 1$ (note that α is represented in linear units, not logarithmic) and a photovoltaic efficiency (γ); $0 < \gamma < 1$ (the percentage of solar energy received which is converted into electrical energy) as shown in Fig. 5. It is dependent on the efficiency of solar cell reduced by the amount of electricity wasted in various conversions (e.g. during switching), a transmittance $\tau = 0$ and a reflectance $\rho = 1 - \alpha$.

Given data:

a. Solar radiation outside the atmosphere is $F_S = 1366$ W/m^2 (solar constant) [24].

1) [b.] Terrestrial albedo is one of the crucial parameter during thermal analysis of a spacecraft [28]–[30]. It is the amount (ratio) of light that is reflected back from

the Earth's surface towards atmosphere without being absorbed. It changes along the Earth's surface and depends on the regional atmosphere and Earth's surface condition (snow, forests, desert, sea etc.). Average terrestrial albedo is slightly lower than 0.4 [28], [29]. Since the AraMiS system is sufficiently close to the earth's surface (say a distance of less than $1/5^{th}$ of the Earth's radius), one can assume that the radiation due to Earth is given by the product of solar radiation by Earth's albedo: $F_T = F_S * 0.4 = 546$ W/m^2 (in fact at a height of 1200 km this is reduced by approximately 70%) [25].

c. The radiation intensity F(T) emitted by a body immersed in vacuum (with a refractive index equal to 1) is given by Stefan-Boltzmann's law [31]:

$$F(T) = \sigma \alpha T^4 \tag{1}$$

where $\sigma = 5.67 \times 10^{-8}$ W/m2.K4 is the Stefan-Boltzmann's constant and α is the absorptance of the surface and T is the absolute temperature.

In reality, the Stefan-Boltzmann law is based on the emissivity of the surface instead of its absorptance, but the Kirchhoff's law [32] states that the two parameters are equal at specific temperature and radiation wavelength.

B. THERMAL EQUATIONS

Since the AraMiS is a closed system, the algebraic sum of the powers that come in any form (radiation and emission) in the system must be equal to the sum of the internal power (converted into chemical energy inside batteries and generated internally by Joule's effect) and the power radiated back to the space. Fig. 4 shows a heat balance for a satellite [33].

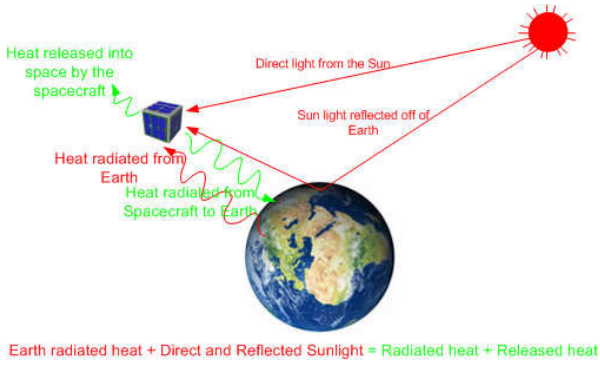

FIGURE 4. Heat balance for a satellite.

Incoming radiation on each face (P_i^S) while assuming solar and terrestrial radiation incident on the same face, is given by:

$$P_i^S = \alpha_i (F_S + F_T) S_i \tag{2}$$

where the subscript i denotes the i^{th} face whose surface is S_i. $F_S = 1366$ W/m^2 is thesolar radiation outside the atmosphere and F_T is the terrestrial radiation. Emitted thermal radiation power from i^{th} face ($P_i^E(T)$) is given by the Stefan-Boltzmann's law:

$$P_i^E(T) = \sigma \alpha_i T^4 S_i \tag{3}$$

Thermal radiation due to the emission from the earth is difficult to assess, but it may be overestimated to get a conservative estimate of the satellite temperature. The following simplified model is used:

- The earth emits thermal radiation due to its surface temperature which can be calculated using Stefan-Boltzmann law (average temperature of earth's surface is 287 K) [31]
- The earth albedo is 0.4 with absorptance α = 1-0.4 = 0.6
- The power density decreases with the square of the distance from the centre of the earth and at an altitude h it is reduced by a factor of $[R/(R+h)]^2$, where R is the radius of the earth. In all these calculations it is assumed that the spacecraft altitude is 800 km
- The face of the satellite parallel to the earth's surface receives all the power density emitted by the earth which is decreased by the absorptance of spacecraft surface and also taking into account the altitude effect
- The sides (perpendicular to the earth surface) get a lower power density and very difficult to estimate. This contribution is overestimated by assuming that each side wall is parallel to the earth's surface (conservative assumption), but receives energy only from half of the earth surface, since the other half is shielded from the rest of the satellite
- The wall of the spacecraft opposite to the earth surface does not receive any energy
- So one can consider an equivalent area of the satellite equal to the sum of the surface facing the earth, plus half of the lateral faces

The above theoretical model can be mathematically expressed as given in (4);

$$\begin{aligned} P^T &= \sigma \alpha_T T_T^4 \left(\frac{R}{R+h}\right)^2 \left(\alpha_{aff} S_{aff} + \alpha_{lat} \frac{S_{lat}}{2}\right) \\ &= F_E \left(\alpha_{aff} S_{aff} + \alpha_{lat} \frac{S_{lat}}{2}\right) \end{aligned} \tag{4}$$

where P^T is the radiated power from the Earth albedo, T_T and α_T are the temperature and absorptance of the Earth respectively, while S_{lat} and S_{aff} are the surfaces areas of the spacecraft facing the ground and the side respectively. While;

$$F_E = \sigma \alpha_T T_T^4 \left(\frac{R}{R+h}\right)^2 \tag{5}$$

where R is the radius of the Earth and h is the altitude of the spacecraft. With previous data, $F_E = 185$ W/m^2;

If it is assumed that solar and terrestrial radiation incident on the same face of the spacecraft, then the power absorbed by the i^{th} face (P_i^P) (while considering the conversion of

light energy into electricity and its chemical storage) is given by (6);

$$P_i^P = \gamma_i(F_S + F_T)S_i \tag{6}$$

Accumulation of heat in the spacecraft due to the heat capacity of the system ($P^C(t)$) is given by (7);

$$P^C(t) = \frac{d}{dt}mcT = mc\frac{d}{dt}T \tag{7}$$

where m is the mass of the system and c is the specific heat.

Let internal heat generation due to electronic circuits be P^J, except for the energy conversion of the panels, that has already been taken into account in the photoelectric efficiency.

The equation of thermal equilibrium can therefore be written as:

$$\sum_{illu\,\min ated\_face}\left(P_i^S - P_i^P\right) - \sum_{remaining\_faces}\left(P_i^E(T)\right) + P^J + P^T - P^C(T) = 0 \tag{8}$$

By inserting values and rearranging (8), the final thermal equilibrium equation is given by (9);

$$\sum_{illu\,\min ated\_face}\left((\alpha_i - \gamma_i)\left(F_S + F_T\right)S_i\right) - \sum_{remaining\_faces}\left(\alpha_i S_i\right)\sigma T^4 + P^J + F_E\left(\alpha_{aff}S_{aff} + \alpha_{lat}\frac{S_{lat}}{2}\right) = mc\frac{d}{dt}T \tag{9}$$

III. SPACECRAFT ANALYSIS UNDER THERMAL EQUILIBRIUM

Let consider various dimension spacecraft's structure in thermal equilibrium under different conditions. These conditions are explained through diverse cases as discussed below.

Case 1: Thermal equilibrium with no generation or accumulation of heat inside the satellite i.e. $dT/dt = 0, P_J = 0$ and $\gamma = 0$.

Let consider some subcases of case 1;

Case 1a: This is the worst case: ''black mirror'', i.e. a thin sheet with one side ideally black ($\alpha = 1$) exposed to solar-terrestrial radiation, and one of the same area, ideally reflecting ($\alpha = 0$) towards the dark.

$$(F_S + F_T + F_E) = \sigma T^4 \tag{10}$$

Therefore, $T = 436.5$ K $= +163.3$ °C (the worst case temperature is very high).

Case 1b: Cube of uniform color (i.e. α equal for all faces), with one face exposed to solar-terrestrial radiation and five faces with same dimensions, are facing the darkness (i.e. one is facing the earth, four are facing sideways):

$$\left(F_S + F_T + F_E\left(1 + \frac{4}{2}\right)\right) = 6\sigma T^4 \tag{11}$$

The temperature, $T = +6.3$ °C.

Case 1c: Solid color cube with two faces exposed to solar-terrestrial radiation (but not orthogonal; let consider the total equivalent area seen from the sun is $\sqrt{2}Si$) and the other faces, obviously of the same surface, facing the dark:

$$\sqrt{2}\left(F_S + F_T\right) + F_E\left(1 + \frac{4}{2}\right) = 6\sigma T^4 \tag{12}$$

The temperature, $T = +22.2$ °C

Case 1d: Cube of uniform color with only one face exposed to the earth radiation and the remaining faces with same dimensions are facing the dark:

$$F_T + F_E\left(1 + \frac{4}{2}\right) = 6\sigma T^4 \tag{13}$$

As the Earth albedo radiation power is negligible, therefore, the spacecraft is almost in dark with an average temperature, $T = -44.7$°C.

Case 1e: Cube of uniform color completely in the dark:

$$F_E\left(1 + \frac{4}{2}\right) = 6\sigma T^4 \tag{14}$$

There is no radiation source and the spacecraft is totally in dark, therefore the resulting average temperature, $T = -80.6$°C.

Case 1f: Planar structure very large compared to the thickness of the spacecraft and uniform color, with one face exposed to solar-terrestrial radiation and other faces with same surface dimension, are facing darkness and having no side walls:

$$F_T + F_E = 2\sigma T^4 \tag{15}$$

The temperature, $T = +58.5$ °C.

Case 1g: Sphere of uniform color with a hemisphere exposed to radiation from solar-terrestrial (but not orthogonal to the surface). Let consider the total ''equivalent'' area seen from the sun equal to the surface of the equatorial circle and the total radiating area equal to 4 times the equatorial surface:

$$(F_S + F_T + F_E) = 4\sigma T^4 \tag{16}$$

The resultant temperature, $T = +18.7$ °C.

Case 2: Consider the spacecraft under thermal equilibrium with uniform color and with internal heat generation.

Then $dT\,/\,dt = 0, P_J > 0$, for uniform color, let $\alpha_i = 0.8$.

Let consider further subcases of case 2;

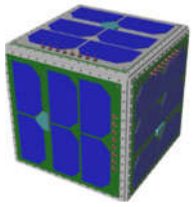

FIGURE 5. ARAMIS satellite with dimension 16.5 × 16.5 × 16.5cm³.

Case 2a: ARAMIS cube of side 16.5cm as shown in Fig. 5, without heat accumulation ($\gamma = 0$), with two faces obliquely

FIGURE 6. ARAMIS satellite with dimension 33 × 33×33cm^3.

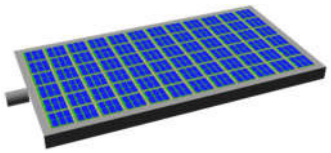

FIGURE 7. ARAMIS tile with dimension 2 × 1m^2.

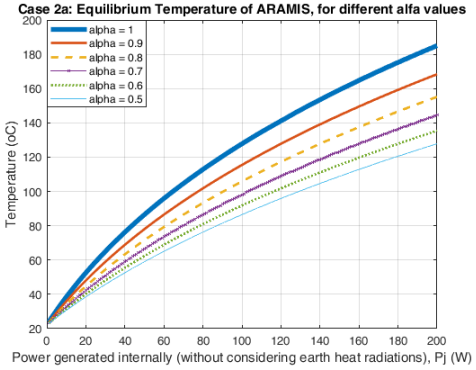

FIGURE 8. ARAMIS temperature without earth heat radiation.

exposed to solar-terrestrial radiation and four faces of the same area, facing the darkness:

$$\sqrt{2}\alpha\left(F_S+F_T\right)+\alpha F_E\left(1+\frac{4}{2}\right)+\frac{P_J}{S}=6\sigma\alpha T^4 \quad (17)$$

The plot of case 2a in Fig. 8 shows the resultant temperature versus the internal power generated (P_J) without considering the earth radiation heat. The plot shows the external temperature radiating from the AraMiS cube surface. Temperature in the inner region will be greater and will depend on the thermal resistance between the point of generation and the outer surface [34].

*Case 2b:*This case is similar to case 2a, but in this case the energy conversion and storage in batteries ($\gamma = 0.23 * 0.8$ i.e. the efficiency of the solar cells multiplied by the efficiency of switching regulator) is also taken into consideration. The temperature can be calculated from the following equation:

$$\sqrt{2}\left(\alpha-\gamma\right)\left(F_S+F_T\right)+\left(\alpha-\gamma\right)F_E\left(1+\frac{4}{2}\right)+\frac{P_J}{S}=6\sigma\alpha T^4 \quad (18)$$

The plot of case 2b in Fig. 9 shows the resultant temperature versus the power generated internally (without

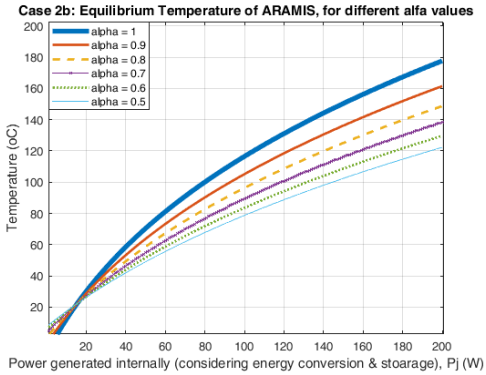

FIGURE 9. ARAMIS temperature due to energy storage.

considering earth heat radiation). This plot provides substantially the maximum power which can continuously be generated inside the satellite, a value between 40W and 70W (for AraMiS satellites), depending on absorptance of the walls and the maximum operating temperature of the system (assumed to be 60 °C).

Case 2c: Similar to case 2b, but for a double ARAMIS structure (33 × 33 cm^2) as shown in Fig. 6 (without considering earth heat radiation).

The plot of case 2c in Fig. 10, provides substantially the maximum power which can continuously be generated inside the satellite, a value between 160 W and 260 W, depending on the absorptance of the walls and maximum operating temperature of the system (assumed to be 60 °C).

Case 2d: Planar structure of ARAMIS tiles (total size 2×1 m^2) as shown in Fig. 7 with single-sided, energy storage $\gamma = 0.23 * 0.8$, a single face exposed to solar-terrestrial radiation and the opposite face of same area, facing the darkness.

$$\sqrt{2}\left(\alpha-\gamma\right)\left(F_S+F_T\right)+\left(\alpha-\gamma\right)F_E\left(1+\frac{4}{2}\right)+\frac{P_J}{S}=2\sigma\alpha T^4 \quad (19)$$

The plot of case 2d in Fig. 11 demonstrates the variation of the power generated internally (without considering earth heat radiation). This plot provides substantially the maximum power which can continuously be generated inside the satellite, a value between 500 W to 600 W which depends on the absorptance of the walls and maximum operating temperature of the system (assumed 60 °C).

Case 3: Transient Analysis: System is not in Thermal Equilibrium i.e. $dT/dt \neq 0$

Thermal equilibrium equation becomes;

$$\sum_{illu\,\min ated\_face}\left(\left(\alpha_i-\gamma_i\right)\left(F_S+F_T\right)S_i\right) - \sum_{all\_faces}\left(\alpha_i S_i\right)\sigma T^4+F_E\left(\alpha_{aff}S_{aff}+\alpha_{lat}\frac{S_{lat}}{2}\right)+P_J = mc\frac{d}{dt}T \quad (20)$$

This is a non-linear first order differential equation.

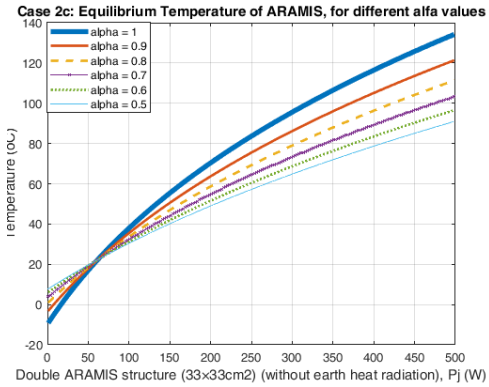

FIGURE 10. ARAMIS satellite temperature due to maximum power generated inside the satellite.

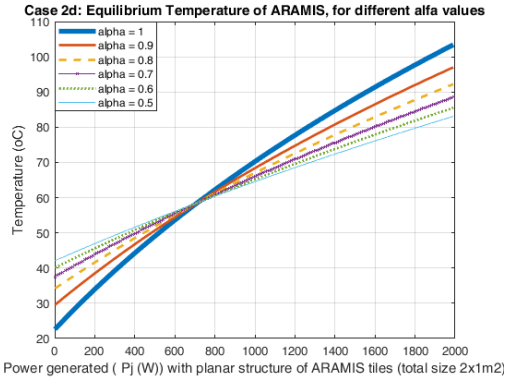

FIGURE 11. ARAMIS tile temperature with planar structure.

Consider the step response to one of the following parameters.

1) Transition of $F_S + F_T$ from 0 to $1366 * 1.4$ W/m^2, and vice versa, that is, the effect of sunrise and sunset.
2) Transition of P_J from 0 to the nominal value and vice versa, that is, powering up and down a generator internal power.
   a) Transition of γ from 0 to $0.23 * 0.8$ and vice versa, that is, powering up and down of a solar panel.

For simplicity, let consider a linearized system whose start and end equilibrium points are known (see cases 1 and case 2 above). Time constant can be calculated as under;

$$\tau = \Theta C \tag{21}$$

where;

$$\frac{1}{\Theta} = \frac{dP}{dT} = \sum_{all\_faces} (\alpha_i S_i)\, \sigma 4T^3$$

While $1/\Theta$ is the thermal resistance for radiation, and $C = mc$ is the heat capacity of the system. Then;

$$\tau = \frac{mc}{\sum\limits_{all\_faces} (\alpha_i S_i)\, \sigma 4T^3} \tag{22}$$

Let consider some sub-cases of case 3.

Case 3a: AraMiS with 6-sided cube and each side with16.5 cm, $\alpha = 0.8$, $m = 5$ kg with aluminum structure (specific heat, $c = 880$ J/kg.K).

Case 3b: Double AraMiS, 6-sided cube of side 33 cm, $\alpha = 0.8$, $m = 50$ kg with aluminum structure.

Case 3c: AraMiS planar structure of 72 dual-sided tiles (2×1 m^2), $\alpha = 0.8$, $m = 500$ kg with aluminum structure.

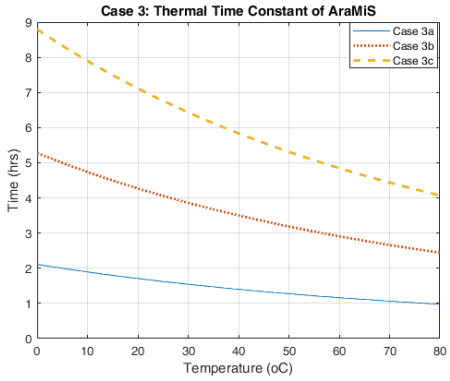

FIGURE 12. Transient analysis of various ARAMIS structures.

The above cases are shown in Fig. 12 (without considering earth heat radiation). It shows that the time constant for structures above the minimum cube (case 3b, 3c) is still higher than the orbital period (about 100 minutes). It can therefore be inferred that the system temperature remains fairly constant at a value intermediate between the two extreme equilibrium points.

*Case 4:*The Realistic Case

Let suppose that the system is exposed for 50% of the time to solar-terrestrial radiation and for the remaining time it is in dark. There is accumulation of energy by the AraMiS, internal dissipation $P_J > 0$ and suppose uniform color of the system with $\alpha_i = 0.8$.

Let consider sub-cases of case 4.

Case 4a: This case is similar to case 2c (here the earth heat radiation are also considered):

Using (18) (including earth heat radiation), the maximum power which can continuously be generated within the structure is then between 210 W and 380 W. This case is plotted in Fig. 13.

Case 4b: This case is similar to case 2d (by considering earth heat radiation):

Using equation 19 (including earth heat radiation), the maximum power which can continuously be generated within the structure is between 1300 W and 2200 W. This case is plotted in Fig. 14.

Case 4c: This case is similar to case 4b but at an altitude of only 200 km (considering the estimation of thermal radiation): This case is plotted in Fig. 15.

Here, it can be observed that the power limits are roughly independent of the altitude in LEO orbits.

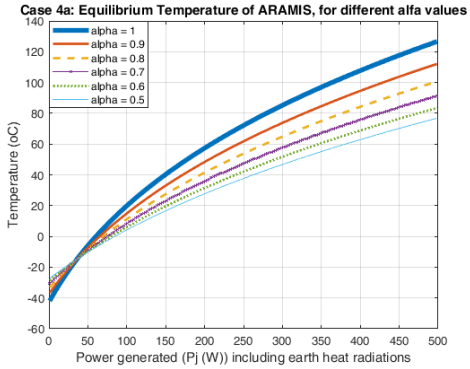

FIGURE 13. ARAMIS satellite temperature including earth heat radiation and internal heat generation 210 W and 380 W.

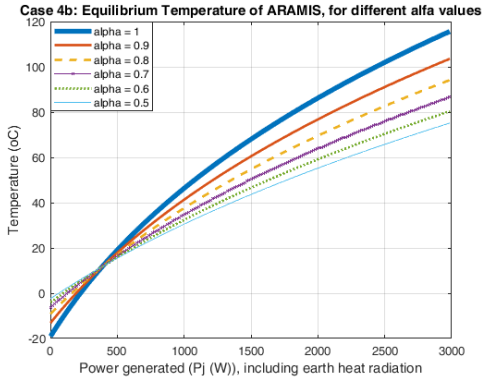

FIGURE 14. ARAMIS satellite temperature including earth heat radiation and internal heat generation 1300 W and 2000 W.

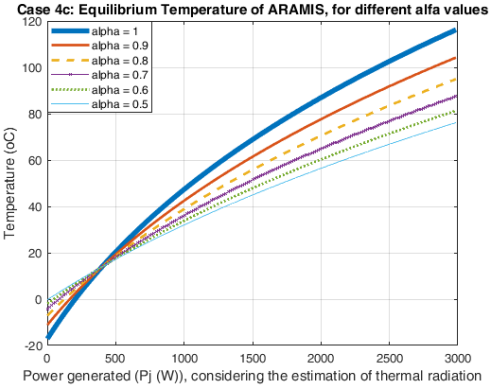

FIGURE 15. Similar to fig. 12 but with and altitude of 1200 km.

So far, all measurements were done for a range of emissivity values (i.e. 0.5 to 0.9). In the next section emissivity of the AraMiS satellite exterior panel is measured through a measurement setup. This emissivity value can be used for accurate temperature and power dissipation measurements of the spacecraft.

IV. ARAMIS SATELLITE EMISSIVITY MEASUREMENT

Emissivity is the relative ability of a material surface to emit energy by radiation. The value of emissivity is dependent on surface color and has a range from 0 to 1. According to Kirchhoff's law of thermal radiation *"for an arbitrary body emitting and absorbing thermal radiation in thermodynamic equilibrium, the emissivity is equal to the absorptivity."* In the following experiments we are going to measure the absorption co-efficient (α) at a specific wavelength and will consider it as emissivity according to Kirchhoff's law [35], [36].

FIGURE 16. Solar simulator for absorption co-efficient measurement.

FIGURE 17. Absorption co-efficient measurement setup.

The absorptivity value of the AraMiS satellite is measured through measurement setups shown in Fig. 16 and Fig. 17. Through these setups, absorptivity is measured by the comparison of solar power absorbed (P_{abs_solar}) and electrical power applied (P_{elect}). Solar power is applied through the setup shown in Fig. 16 and same amount of electrical power is applied through the setup shown in Fig. 16. The two powers are compared as shown in equation (23).

$$\begin{aligned} P_{abs\_solar} &= P_{elect} \\ \alpha F_S.S &= V.I \\ \alpha &= \frac{V.I}{F_S.S} \end{aligned} \tag{23}$$

where P_{abs_solar} is the solar power absorbed, P_{elec} is the electrical power applied, F_S is the solar power density (i.e. 1366 W/m^2, α is the absorption co-efficient, S is the solar panel surface area, V is the applied voltage and I is the current flowing through the air coil.

In the first setup of this measurement as shown in Fig. 16, solar panel module was illuminated through a solar simulator.

A solar simulator is an instrument that can deliver natural sunlight at various intensity levels. The purpose of the solar simulator here is to provide a controllable natural sunlight at *AM0* intensity. The corresponding temperature rise was noted using a temperature sensor. When the corresponding temperature reached a steady state value (70 °C), the temperature was recorded and the solar simulator was switched off. Through next setup shown in Fig. 17, electrical power will be applied to the solar panel module and the corresponding temperature will be increased to 70 °C (equivalent to solar power temperature rise). The two powers will be compared and emissivity will be measured as given in (23).

In the second measurement setup, the AraMiS solar panel module is placed inside the vacuum chamber as shown in Fig. 17. Electrical power is applied to the embedded air coil of the solar panel module. The air coil dissipated heat corresponding to the applied power and the solar panel module surface temperature started increasing and after sometime it achieved a steady state value. The applied power is increased to raise the surface temperature to 70 °C (equivalent to solar power). The applied voltage, the corresponding current flowing through the coil and the resulting temperature has been acquired through data acquisition system and plotted as shown in Fig. 18.

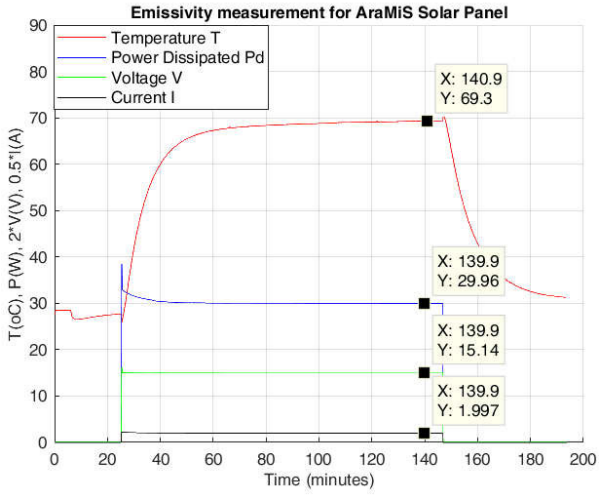

FIGURE 18. AraMiS solar panel absorption co-efficient measurement data.

By inserting the required values in equation (23) from table 1, the emissivity value measured for AraMiS solar panel is 0.86. Using this emissivity value, the exact value of equilibrium temperature of AraMiS can be found for all the cases given in Fig. 8 ∼ Fig. 15.

V. SATELLITE SPIN ANALYSIS LED BY A GRADIENT OF COLOR

This section of the paper presents a preliminary analysis of an AraMiS dimension system in relation to the spin induced by the color (absorptance) asymmetry of the outer surface of the satellite, considering substantial contributions of:

- Solar radiation and the Earth's albedo
- Absorptance difference on both sides of the bright faces
- Moment of inertia of the satellite

In space system, due to color (absorptance) difference between opposite edges, solar flux pressure is greater on one edge as compared to the other. As there is no friction in space, this delta in solar flux generates a pressure difference exerted on the spacecraft opposite edges and results in spacecraft spinning [37].

TABLE 1. Parameters for emissivity measurement.

Parameter	Value
Room temperature (*TI*)	292 K
Solar panel steady state surface temperature (To) at P_{elec} = 80 W	343 K
Solar panel surface area (*S*)	0.0256 m^2
Power applied to embedded air coil (P_{elect})	30 W
Solar power density	1366 W/m^2

A. PRECONDITIONS

Let consider a system composed of N square faces of side L, adjacent to one another, arranged in a plane illuminated perpendicularly. Each face is characterized by a uniform absorptance on all surfaces except on two symmetrical strips of width D, posed to the opposing edges whose absorptance are α_1 and α_2 respectively as shown in Fig. 19.

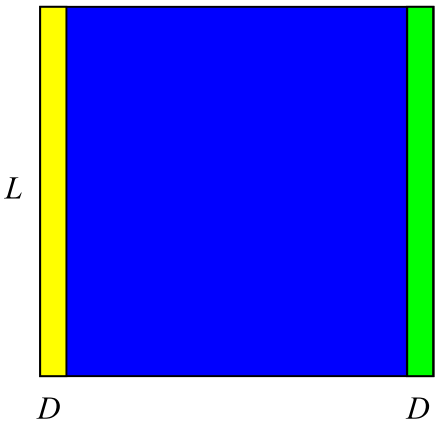

FIGURE 19. System composed of N square faces of side L.

Let the system have zero photoelectric efficiency $\gamma = 0$ (i.e. all solar panels are off), a transmittance $\tau = 0$ (non-transparent surface) and a reflectance $\rho = 1\text{-}\alpha$.

Given data:

- Solar radiation outside the atmosphere is F_S = 1366 W/m^2 (solar constant).
- It can be assumed that the radiation due to Earth is given approximately by the product of solar radiation with the

Earth's albedo $F_T = F_S * 0.4 = 546$ W/m^2 (at a height of 1200 km this is reduced by 70% approximately).

- The radiation pressure of sun light reflected from the Earth, for a non-transparent body is given by:

$$p = \frac{F_S + F_T}{c}(2 - \alpha) \tag{24}$$

where, $c = 2.998 \times 10^8$ m/s is the speed of light.

B. ANALYSIS OF THE MECHANICAL MOMENTUM AND THE SPIN-INDUCED

Let consider the following formulas:

- The radiation pressure on the central face creates no momentum with respect to the center of the face as the absorptance is uniform and the system is symmetric about its geometric center.
- The force acting on each of the two side rails will be given by the product of pressure to the surface of each colored rail, respectively as given by (25);

$$F_1 = \frac{F_S + F_T}{c}(2 - \alpha_1)\, LD$$
$$F_2 = \frac{F_S + F_T}{c}(2 - \alpha_2)\, LD \tag{25}$$

- While the moment (M) of these two forces imposed on the geometric center of each rail is given by their difference multiplied by the distance between the points of application as given by (26).

$$M = \frac{F_S + F_T}{c}(\alpha_2 - \alpha_1)\, LD\,(L - D) \tag{26}$$

- The angular acceleration due to sum of N of these moments (as there are so many faces) is given by (27).

$$\dot{\omega} = N\frac{M}{J} \tag{27}$$

where J is the moment of inertia with respect to the axis of rotation, assuming for simplicity the tensor of inertia is diagonal (i.e. the momentum along one axis does not generate rotations along axes perpendicular to it).

- The time required to rotate the satellite, initially without spin, with an angular velocity ω_0 is given by (28).

$$T = \frac{\omega_0}{\dot{\omega}} = \frac{\omega_0 J}{NM} \tag{28}$$

- The moment of inertia is considered for a uniformly filled sphere of radius r and mass m as given by (29).

$$J = \frac{3mr^2}{5} \tag{29}$$

C. EXAMPLES

Let consider some cases of various AraMiS satellite architectures and apply the above analysis to measure the moment of inertia and time of rotation for a single spin.

- **Case 1:** AraMiS, cube minimum: Consider AraMiS satellite with $N = 1$, $L = 150$ mm (side of the PCB), $D = 20$ mm, α_2 - $\alpha_1 = 0.3$ (i.e. gradient of color that is considered very high), $m = 5$ kg, $r = 220$ mm.
- **Case 2:** AraMiS, double cube: Consider AraMiS satellite with $N = 4$, $L = 150$ mm (side of the PCB), $D = 20$ mm, α_2 - $\alpha_1 = 0.3$ (i.e. gradient of color that is considered very high), $m = 50$ kg, $r = 440$ mm.
- **Case 3:** AraMiS, cube six times: Consider AraMiS satellite with $N = 36$, $L = 150$ mm (side of the mould), $D = 20$ mm, α_2 - $\alpha_1 = 0.3$ (i.e. gradient of color that is considered very high), $m = 500$ kg, $r = 1320$ mm.

Table 2 provides the results to arrive at a rotation $\omega = 1$ rpm.

TABLE 2. Momentum and time of rotation for various AraMiS satellite architectures.

Cases	Momentum, M (Nm^2)	Time of rotation, T (years)
Case 1	0.75e^{-9}	0.58
Case 2	0.75e^{-9}	5.85
Case 3	0.75e^{-9}	58

VI. CONCLUSION

The paper discussed in detail the thermal analysis technique of small satellites considering all the possible heat sources in space environment. Small satellites of various dimensions are analyzed for five heat sources which were explained through different cases. In case 1, it was considered that the satellite system is in thermal equilibrium with no generation or accumulation of heat. Case 1 was further divided into seven sub-cases with various conditions and the resultant temperature is measured. In case 2 the spacecraft was considered under thermal equilibrium with internal heat generation. As contrary to previous two cases, in case 3, the spacecraft was analyzed under transient conditions. In case 4, the spacecraft was analyzed for a realistic case that the system is exposed for 50% of the time to solar-terrestrial radiation and for the remaining time it is in dark. There is accumulation of energy inside the system and the system is also dissipating heat internally. The four cases results were plotted for a range of emissivity values (i.e. 0.5 to 1). In the next section emissivity of the AraMiS satellite exterior panel is measured through an experimental setup. This emissivity value can be used for accurate temperature and power dissipation measurements of the satellite.

In the last section of the paper, the satellite spin was analyzed for the color gradient. Three cases of AraMiS architecture with various dimensions and weight are analyzed for the momentum and rotation time due to color gradient with an absorptance difference of 0.3. The analysis shows that the satellite will complete two extra spins per year due to color gradient. Increase in absorption difference will result in higher spin rate.

REFERENCES

[1] S. Speretta, M. L. Reyneri, C. Sansoe, M. Tranchero, C. Passerone, and D. D. Corso, "Modular architecture for satellites," in *Proc. 58th IAC*, Hyderabad, India, Sep. 2007, pp. 24–28.
[2] Z. Qu, G. Zhang, H. Cao, and J. Xie, "LEO satellite constellation for Internet of Things," *IEEE Access*, vol. 5, pp. 18391–18401, 2017, doi: 10.1109/ACCESS.2017.2735988.
[3] R. Munakata, *CubeSat Design Specifications, Rev.12*, Pomona, CA, USA: California State Polytechnic Univerity, 2009.
[4] L. Alminde, M. Bisgaard, D. Vinther, T. Viscor, and K. Ostergard, "Educational value and lessons learned from the AAU-CubeSat project," in *Proc. Int. Conf. Recent Adv. Space Technol. RAST*, Nov. 2003, pp. 57–62.
[5] J. C. D. L. Rios, D. Roascio, L. Reyneri, C. Sansoè, C. Passerone, D. D. Corso, M. Bruno, A. Hernandez, and A. Vallan, "ARAMIS: A fine-grained modular architecture for reconfigurable space missions," in *Proc. 1st Conf. Univ. Satell. Missions*, Jan. 2011.
[6] M. R. Mughal, J. C. De Los Rios, L. M. Reyneri, and A. Ali, "Scalable plug and play tiles for modular nanoSatellites," in *Proc. 63rd Int. Autronautical Congr.*, Naples Italy, Oct. 2012, pp. 1–5.
[7] M. R. Mughal, A. Ali, and M. L. Reyneri, "Plug-and-play design approach to smart harness for modular small satellites," *Acta Astronautica*, vol. 94, no. 2, pp. 754–764, Feb. 2014, doi: 10.1016/j.actaastro.2013.09.015.
[8] A. Ali, M. L. Reyneri, J. C. de los Rios, and H. Ali, "Innovative power management tile for nanoSatellites," in *Proc. 63rd Int. Autronautical Congr.*, Naples Italy, Oct. 2012, pp. 1–5.
[9] A. Ali, M. R. Mughal, H. Ali, and L. Reyneri, "Innovative power management, attitude determination and control tile for CubeSat standard NanoSatellites," *Acta Astronautica*, vol. 96, pp. 116–127, Mar. 2014, doi: 10.1016/j.actaastro.2013.11.013.
[10] A. Ali, L. Reyneri, J. C. de los Rios, H. Ali, and M. R. Mughal, "Reconfigurable magnetorquer for the CubePMT module of CubeSat satellites," in *Proc. 15th Int. Multitopic Conf. (INMIC)*, Dec. 2012, pp. 178–183.
[11] M. Barreiro and A. Diego, "A small satellite preliminary thermal control and heat shield analysis," M.S. thesis, MIT, Cambridge, MA, USA, Feb. 2008.
[12] K. F. C. H. Sam and Z. Deng, "Optimization of a space based radiator," *Appl. Thermal Eng.*, vol. 31, nos. 14–15, pp. 2312–2320, Oct. 2011.
[13] K. Yamada and H. Nagano, "Development of a heat storage panel for micro/nano-satellites and demonstration in orbit," *Appl. Thermal Eng.*, vol. 91, pp. 894–900, Dec. 2015.
[14] M. U. Carfi and B. B. Dogan, "A comparative thermal study of a GEO satellite for geostationary transfer orbit and mission orbit," in *Proc. 9th Int. Conf. Recent Adv. Space Technol. (RAST)*, Jun. 2019, pp. 329–333.
[15] A. Ali, "Power management, attitude determination and control systems of small satellites," Ph.D. dissertation, Dept. Electron. Telecommun., Politecnico di Torino, Turin, Italy. [Online]. Available: http://porto.polito.it/2535715/
[16] K. Hogstrom, "State-of-the-art thermal analysis methods and validation for small spacecraft," *Ae241 Literature Surv.*, 2013.
[17] S. Arabaci and E. Dirgin, "Thermal mathematical model correlation of an Earth observation satellite," in *Proc. 7th Int. Conf. Recent Adv. Space Technol. (RAST)*, Jun. 2015, pp. 439–442.
[18] M. A. Gadalla, "Prediction of temperature variation in a rotating spacecraft in space environment," *Appl. Thermal Eng.*, vol. 25, nos. 14–15, pp. 2379–2397, Oct. 2005.
[19] A. Grams, B. Curran, S. Kuttler, J. Reyes, F. Wist, and K.-D. Lang, "Thermal management of a ka band satellite communication module using finite element models and thermal imaging," in *Proc. 24rd Int. Workshop Thermal Investigations ICs Syst. (THERMINIC)*, Sep. 2018, pp. 1–4.
[20] J.-R. Tsai, "Overview of satellite thermal analytical model," *J. Spacecraft Rockets*, vol. 41, no. 1, pp. 120–125, Jan. 2004.
[21] A. Farrahi and I. Pérez-Grande, "Simplified analysis of the thermal behavior of a spinning satellite flying over sun-synchronous orbits," *Appl. Thermal Eng.*, vol. 125, pp. 1146–1156, Oct. 2017.
[22] C. A. Gueymard, "A reevaluation of the solar constant based on a 42-year total solar irradiance time series and a reconciliation of spaceborne observations," *Sol. Energy*, vol. 168, pp. 2–9, Jul. 2018, doi: 10.1016/j.solener.2018.04.001.
[23] N. D. Anh, N. N. Hieu, P. N. Chung, and N. T. Anh, "Thermal radiation analysis for small satellites with single-node model using techniques of equivalent linearization," *Appl. Thermal Eng.*, vol. 94, pp. 607–614, Feb. 2016.
[24] Z. Song, S. Liang, D. Wang, Y. Zhou, and A. Jia, "Long-term record of top-of-atmosphere albedo over land generated from AVHRR data," *Remote Sens. Environ.*, vol. 211, pp. 71–88, Jun. 2018.
[25] Y. Song, X. Wang, S. Bi, J. Wu, and S. Huang, "Effects of solar radiation, terrestrial radiation and lunar interior heat flow on surface temperature at the nearside of the moon: Based on numerical calculation and data analysis," *Adv. Space Res.*, vol. 60, no. 5, pp. 938–947, Sep. 2017.
[26] A. Elghool, F. Basrawi, T. K. Ibrahim, K. Habib, H. Ibrahim, and D. M. N. D. Idris, "A review on heat sink for thermo-electric power generation: Classifications and parameters affecting performance," *Energy Convers. Manage.*, vol. 134, pp. 260–277, Feb. 2017.
[27] T. Y. Kim, "Heat capacity estimation of the thermal buffer mass for temperature control of satellite electronic components in periodic operation," *Aerosp. Sci. Technol.*, vol. 30, no. 1, pp. 286–292, Oct. 2013.
[28] B. Zhang, L. Lei, X. Zhou, and L. Zhang, "Change assessment of albedo for different humanistic regions," in *Proc. IEEE Int. Geosci. Remote Sens. Symp.*, Jul. 2010, pp. 887–890, doi: 10.1109/IGARSS.2010.5651001.
[29] Z. Wang, Q. Qin, Y. Sun, G. Han, and H. Ren, "Retrieval of surface albedo based on BRDF model," in *Proc. IEEE Int. Geosci. Remote Sens. Symp. IGARSS*, Jul. 2018, pp. 8949–8952, doi: 10.1109/IGARSS.2018.8518775.
[30] T. He, S. Liang, D. Wang, Q. Shi, and X. Tao, "Estimation of high-resolution land surface shortwave albedo from AVIRIS data," *IEEE J. Sel. Topics Appl. Earth Observ. Remote Sens.*, vol. 7, no. 12, pp. 4919–4928, Dec. 2014, doi: 10.1109/JSTARS.2014.2302234.
[31] M. Wellons, "The Stefan–Boltzmann law," Dept. Phys., College Wooster, Wooster, OH, USA, May 2007.
[32] R. Zevenhoven, M. Fält, and L. P. Gomes, "Thermal radiation heat transfer: Including wavelength dependence into modeling," *Int. J. Thermal Sci.*, vol. 86, pp. 189–197, Dec. 2014.
[33] *Heat Balance Photo*. Accessed: Jan. 8, 2020. [Online]. Available: http://www.qrg.northwestern.edu/projects/vss/docs/thermal/2-what-is-heat-balance.html
[34] A. Ali, K. Ullah, H. U. Rehman, I. Bari, and L. M. Reyneri, "Thermal characterisation analysis and modelling techniques for CubeSat-sized spacecrafts," *Aeronaut. J.*, vol. 121, no. 1246, pp. 1858–1878, Dec. 2017, doi: 10.1017/aer.2017.108.
[35] S. Cao, X. Chen, G. Wu, J. Yang, R. Wang, S. Kaiwen, and L. Wang, "Variable emissivity surfaces for micro and nano-satellites," *Phys. Procedia*, vol. 18, pp. 91–94, Jan. 2011.
[36] R. J. Howell, R. Siegel, and M. P. Mengüc, *Thermal Radiation Heat Transfer*, 5th ed. Boca Raton, FL, USA: CRC Press, 2013.
[37] M. A. Earl, P. W. Somers, K. Kabin, D. Bédard, and G. A. Wade, "Estimating the spin axis orientation of the Echostar-2 box-wing geosynchronous satellite," *Adv. Space Res.*, vol. 61, no. 8, pp. 2135–2146, Apr. 2018.

ANWAR ALI received the B.E. degree in electronics engineering from the NED University of Engineering and Technology (UET), Karachi, Pakistan, in 2004, and the M.S. degree in electronic engineering and the Ph.D. degree in electronics and communication engineering from the Politecnico di Torino, Italy, in 2010 and 2014, respectively. He is currently working as an Associate Professor with the School of Information Science and Technology, Zhejiang Sci-Tech University, Hangzhou, China. His research interests include design and development of power management, attitude determination and control subsystems of small satellites, electronic system design, power electronics applications, analog electronics and thermal analysis, and thermal modeling of aerospace systems.

JIJUN TONG was born in September 1977. He received the B.S., M.S., and Ph.D. degrees in biomedical engineering from Zhejiang University, in 1999, 2003, and 2008, respectively.

He is currently a Professor with Zhejiang Sci-Tech University, where he is also a master's tutor. His research interests include medical big data, medical image and signal processing, embedded systems, and instrumentation.

HAIDER ALI (Senior Member, IEEE) was born in 1984. He received the B.S. degree in telecommunication engineering from the National University of Computer and Emerging Sciences (NUCES), Pakistan, in 2007, and the M.S. degree in electronics engineering and the Ph.D. degree in electronics and communication engineering from the Politecnico di Torino, Italy, in 2010 and 2014, respectively.

He is currently working as an Assistant Professor with the Department of Electrical and Electronics Engineering, University of Technology, Nowshera, Pakistan. His research interests include design and development of antennas, the radio frequency front end and telecommunication subsystems for nano- and picosatellites, smart grids, power electronics, and electronic system design.

MUHAMMAD RIZWAN MUGHAL was born in Chakwal, Pakistan, in 1985. He received the B.S. degree (Hons.) in electrical engineering from the University of Engineering and Technology (UET), Taxila, Pakistan, in 2007, and the Ph.D. degree in electronics and communication engineering from the Politecnico di Torino, Italy, in March 2014.

Since June 2014, he has been an Assistant Professor with the Department of Electrical Engineering, Institute of Space Technology, Islamabad, Pakistan. Since July 2018, he has been associated with the Department of Electronics and Nanoengineering, Aalto University, Finland. His research interests include plug-and-play design and smart communication solutions for satellites, wireless solutions for intrasatellite data communication, and satellite's testing methodologies.

LEONARDO M. REYNERI received the M.Sc. degree *(cum laude)* from the Politecnico di Torino, Italy, in 1984, and the Ph.D. degree, in 1992.

He is currently a Full Professor with the Department of Electronics and Telecommunications, Politecnico di Torino. He has been working, since more than 20 years, on the development of tools and methods for co-design and co-simulation of HW/SW and mixed-signal systems. He is one of the developers of the AraMiS Architecture. His current research interests include the design of low-cost space systems and modular micro and minisatellites for surveillance, environmental monitoring, and disaster management.